Coherent vortex extraction in three-dimensional homogeneous turbulence: Comparison between CVS-wavelet and POD-Fourier decompositions

Marie Farge[a)]
LMD-IPSL-CNRS, Ecole Normale Supérieure, 24 rue Lhomond, 75231 Paris Cedex 05, France

Kai Schneider
CMI, Université de Provence, 39 rue Joliot-Curie, 13453 Marseille Cedex 13, France and L3M-CNRS, IMT, 38 rue Joliot-Curie, 13451 Marseille Cedex 20, France

Giulio Pellegrino
L3M-CNRS, IMT, 38 rue Joliot-Curie, 13451 Marseille Cedex 20, France

Alan A. Wray and Robert S. Rogallo
NASA-Ames Research Center, Moffett Field, California 94035

(Received 22 November 2002; accepted 21 May 2003; published 2 September 2003)

The coherent vortex simulation (CVS) decomposes each realization of a turbulent flow into two orthogonal components: An organized coherent flow and a random incoherent flow. They both contribute to all scales in the inertial range, but exhibit different statistical behaviors. The CVS decomposition is based on the nonlinear filtering of the vorticity field, projected onto an orthonormal wavelet basis made of compactly supported functions, and the computation of the induced velocity field using Biot–Savart's relation. We apply it to a three-dimensional homogeneous isotropic turbulent flow with a Taylor microscale Reynolds number $R_\lambda = 168$, computed by direct numerical simulation at resolution $N = 256^3$. Only 2.9%N wavelet modes correspond to the coherent flow made of vortex tubes, which contribute 99% of energy and 79% of enstrophy, and exhibit the same $k^{-5/3}$ energy spectrum as the total flow. The remaining 97.1%N wavelet modes correspond to a incoherent random flow which is structureless, has an equipartition energy spectrum, and a Gaussian velocity probability distribution function (PDF). For the same flow and the same compression rate, the proper orthogonal decomposition (POD), which in this statistically homogeneous case degenerates into the Fourier basis, decomposes each flow realization into large scale and small scale flows, in a way similar to large eddy simulation (LES) filtering. It is shown that the large scale flow thus obtained does not extract the vortex tubes equally well as the coherent flow resulting from the CVS decomposition. Moreover, the small scale flow still contains coherent structures, and its velocity PDF is stretched exponential, while the incoherent flow is structureless, decorrelated, and its velocity PDF is Gaussian. Thus, modeling the effect of the incoherent flow discarded by CVS-wavelet shall be easier than modeling the effect of the small scale flow discarded by POD-Fourier or LES. © *2003 American Institute of Physics.* [DOI: 10.1063/1.1599857]

I. INTRODUCTION

Since the work presented in this paper has been performed at NASA-Ames during the CTR (Center for Turbulence Research) Summer Program 2000,[1] we recall the comments on turbulence research made in 1948 by Hugh L. Dryden, the first director of NACA (later NASA).

Dryden begins his paper on "Recent advances in the mechanics of boundary layer flow"[2] by stating: "*There have been no notable advances in the theory of fully developed turbulent motion during the last decade.... In the period 1934–1938 Taylor developed his statistical theory of turbulence, which was so fruitful in treating the problem of isotropic turbulence. Von Kármán extended the theory, clothed it in more elegant mathematical form, and attempted, with incomplete success, to treat the problem of shear flow.... At the Fifth International Congress of Applied Mechanics in 1938... Tollmien and Prandtl suggested that the turbulent fluctuations might consist of two components, one derivable from a harmonic function and the other satisfying an equation of the heat conduction type, i.e., a nondiffusive and a diffusive component, or viscosity independent and viscosity dependent type.*"

Tollmien and Prandtl's suggestion to split the turbulent fluctuations into non-diffusive and diffusive components is very similar to the concept behind coherent vortex simulation (CVS) which we introduced in Refs. 3–5. CVS tracks the nonlinear dynamics (the non-diffusive component) using an adaptive wavelet basis,[6–8] which captures the coherent vortices at all scales, and discards the incoherent background flow (the diffusive component) which has reached a statistical equilibrium characterized by a Gaussian velocity prob-

[a)]Author to whom correspondence should be addressed. Telephone: +33 1 44 32 22 35; fax: +33 1 43 36 83 92. Electronic mail: farge@lmd.ens.fr

ability distribution function (PDF) and an energy equipartition spectrum.[3,5,9]

Later, Dryden adds: "*The mixing length concept seems wholly inadequate..., the "mean free path," mixing length, or scale of the turbulent processes is large compared with the thickness of the boundary layer. Considerable masses of fluid move as more or less coherent units. The process cannot be smoothed by averaging over a small volume because it is not possible to choose dimensions small compared with a single fluid element. The mixing length idea, that the turbulent fluctuations and the turbulent shear stress are directly related to the mean speed at a point and its derivatives at that point, must be abandoned. Shall the flow then be regarded as a mean flow that merely transports and distorts large eddies superposed on the flow, these eddies being of varying size and intensity*?"

This comment of Dryden, which assumes that turbulent flows are composed of coherent units of varying sizes and intensities which cannot be smoothed by averaging, supports our proposal of using the wavelet representation to study turbulent flows.[10] We have shown with the continuous wavelet transform that coherent vortices are multiscale eddies whose activity covers the entire inertial range and induces the intermittency of turbulent flows.[11,12] We confirmed this with the orthogonal wavelet transform,[3] and demonstrated that coherent vortex tubes are responsible for the $k^{-5/3}$ energy spectrum of 3D turbulent flows.[9,13]

Finally Dryden concludes: "*The rapidly developing theory of random functions*[14] *may possibly form the mathematical framework of an improved theory of turbulence. However it is necessary to separate the random processes from the non-random processes. It is not yet fully clear what the random elements are in turbulent flows. The experimental results described suggest that the ideas of Tollmien and Prandtl, that the measured fluctuations include both random and non-random elements, are correct, but as yet there is no known procedure either experimental or theoretical for separating them*."

The CVS decomposition proposes such a procedure. We developed it over the last ten years[1,3,5,9,10,15] in order to separate the turbulent fluctuations into organized and random components. In 1992[15] we found that the nonlinear dynamics of two-dimensional turbulent flows, and therefore, their predictability, is better preserved by compressing the flow using a wavelet packet basis rather than a Fourier basis. In 1994[16] we showed that a wavelet packet basis is also better suited for this than adapted local cosine bases, which correspond to wave packets. In 1999[3] we selected the wavelet basis as the optimal basis for the CVS decomposition of turbulent flows. Similarly to the wavelet methods developed for signal denoising,[17,18] the CVS decomposition is based on a nonlinear filtering of the vorticity field projected onto an orthonormal wavelet basis made of compactly supported functions. The corresponding organized and random components of the velocity field are reconstructed using Biot–Savart's relation.

We apply the CVS decomposition to a 3D statistically stationary homogeneous isotropic turbulent flow with a Taylor microscale Reynolds number $R_\lambda = 168$, which has been computed by direct numerical simulation (DNS) at resolution $N = 256^3$. The choice of a statistically stationary homogeneous isotropic flow is made on purpose, to demonstrate the efficiency of the CVS simulation in the worst possible case for it. Indeed, the wavelet representation used by CVS is better suited to treat nonstationary or inhomogeneous flows rather than stationary or homogeneous flows.[13,19]

In Ref. 20 another wavelet method, based on a two-dimensional cut of the velocity field, has been proposed to decompose experimental data of a turbulent mixing layer into coherent structures and background fluctuations. In Ref. 21 different techniques for extracting coherent structures in experimental data of turbulent shear flows have been reviewed, including proper orthogonal decomposition (POD) and wavelet methods. In Ref. 13 we have applied the CVS decomposition to DNS data of a 3D time developing turbulent mixing layer and in Ref. 19 of a 3D turbulent jet in a stratified flow modeling the atmospheric tropopause.

In this paper we compare the coherent vortices extracted by the CVS decomposition with those obtained after filtering the vorticity field using the POD for the same number of retained modes. Since the flow studied here is statistically invariant by translation and rotation, in this case the POD degenerates into the Fourier basis, where the modes are sorted in increasing order of the wavenumber. Such a homogeneous isotropic flow is the most difficult case to treat for both POD and CVS, but it is the most generic turbulent flow one can compute at large Reynolds numbers without any *ad hoc* turbulence model.

II. CVS DECOMPOSITION

A. Wavelet projection

We consider a 3D vorticity field $\boldsymbol{\omega}(\boldsymbol{x}) = \nabla \times \boldsymbol{V}(\boldsymbol{x})$, computed with resolution $N = 2^{3J}$, N being the number of grid points and J the number of octaves in each direction. The three components $\omega_n(\boldsymbol{x})$, with $n = 1, 2, 3$, are developed into an orthonormal wavelet series, from the largest scale $l_{\max} = 2^0$ and to the smallest scale $l_{\min} = 2^{-J+1}$, using a 3D multiresolution analysis (MRA)[10,22]

$$\omega_n(\boldsymbol{x}) = [\overline{\omega}_{0,0,0}]_n \phi_{0,0,0}(\boldsymbol{x}) + \sum_{j=0}^{J-1} \sum_{i_x=0}^{2^j-1} \sum_{i_y=0}^{2^j-1} \sum_{i_z=0}^{2^j-1} \sum_{\mu=1}^{7} [\tilde{\omega}^{\mu}_{j,i_x,i_y,i_z}]_n \psi^{\mu}_{j,i_x,i_y,i_z}(\boldsymbol{x}).$$

The 3D orthogonal scaling functions are

$$\phi_{j,i_x i_y,i_z}(\boldsymbol{x}) = \phi_{j,i_x}(x)\,\phi_{j,i_y}(y)\,\phi_{j,i_z}(z),$$

and the corresponding 3D orthogonal wavelets are

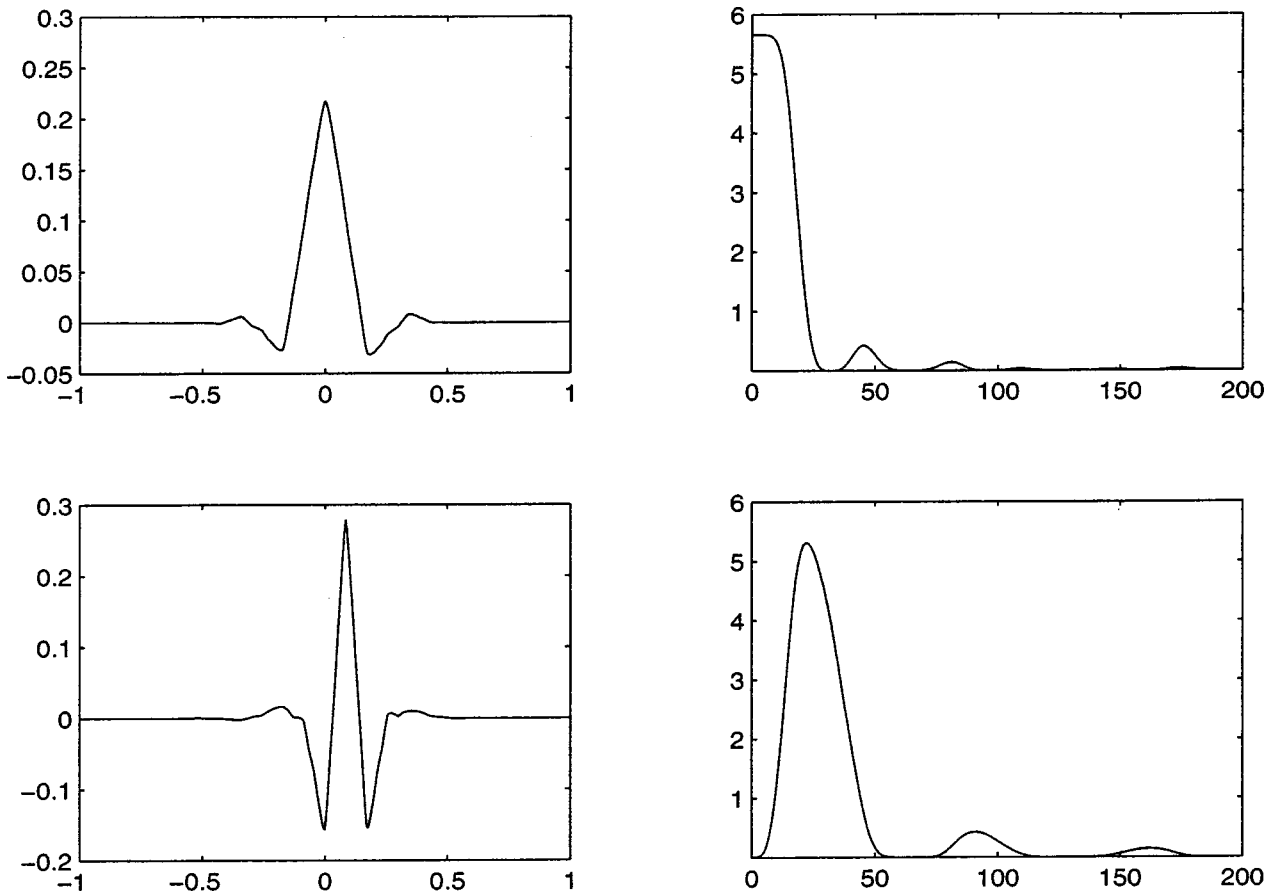

FIG. 1. Coiflet 12 wavelet: The scaling function ϕ (top) and the corresponding wavelet ψ (bottom), in physical space (left) and their corresponding moduli, $|\hat{\phi}|$ and $|\hat{\psi}|$, in Fourier space (right).

$$\psi^{\mu}_{j,i_x,i_y,i_z}(\boldsymbol{x}) = \begin{cases} \psi_{j,i_x}(x)\phi_{j,i_y}(y)\phi_{j,i_z}(z); & \mu=1, \\ \phi_{j,i_x}(x)\psi_{j,i_y}(y)\phi_{j,i_z}(z); & \mu=2, \\ \phi_{j,i_x}(x)\phi_{j,i_y}(y)\psi_{j,i_z}(z); & \mu=3, \\ \psi_{j,i_x}(x)\phi_{j,i_y}(y)\psi_{j,i_z}(z); & \mu=4, \\ \psi_{j,i_x}(x)\psi_{j,i_y}(y)\phi_{j,i_z}(z); & \mu=5, \\ \phi_{j,i_x}(x)\psi_{j,i_y}(y)\psi_{j,i_z}(z); & \mu=6, \\ \psi_{j,i_x}(x)\psi_{j,i_y}(y)\psi_{j,i_z}(z); & \mu=7. \end{cases}$$

Here $\phi_{j,i}$ is a one-dimensional scaling function and $\psi_{j,i}$ the corresponding one-dimensional wavelet, j the index for the scale discretization, i_x, i_y, i_z the indices for the space discretization and μ the index for the seven discrete directions in 3D space. Due to orthogonality, the scaling coefficients are given by $[\overline{\omega}_{0,0,0}]_n = \langle \omega_n, \phi_{0,0,0} \rangle$ and the wavelet coefficients by $[\tilde{\omega}^{\mu}_{j,i_x,i_y,i_z}]_n = \langle \omega_n, \psi^{\mu}_{j,i_x,i_y,i_z} \rangle$, where $\langle \cdot, \cdot \rangle$ denotes the L^2-inner product.

We have chosen Coifman 12 wavelets,[22] because they are almost symmetric, which is not the case for Daubechies wavelets. They are compactly supported functions (Fig. 1, bottom) with $M=4$ vanishing moments, which are computed using a quadrature mirror filter of length $3M=12$. The corresponding scaling function (Fig. 1, top) has also M vanishing moments (except the zeroth-order moment).

The CVS decomposition algorithm consists of three fast wavelet transforms, one for each vorticity component, a thresholding of the wavelet coefficients, and three inverse fast wavelet transforms to reconstruct the coherent vorticity. The incoherent vorticity is then obtained by substracting the coherent from the total vorticity, as the wavelet transform is linear. The computational cost of the fast wavelet transform is of order CN, where N is the resolution, and C is proportional to the filter length $3M$, with $M=4$ for the Coifman 12 wavelet used here. Therefore, the total number of operations is $O(N)$, while it is $O(N \log_2 N)$ for the fast Fourier transform (FFT).

B. Nonlinear thresholding

The vorticity field is decomposed into coherent vorticity $\boldsymbol{\omega}_C(\boldsymbol{x})$ and incoherent vorticity $\boldsymbol{\omega}_I(\boldsymbol{x})$ by projecting its three components onto an orthonormal wavelet basis and applying nonlinear thresholding to the wavelet coefficients. The choice of the threshold is based on theorems[17,18] proving optimality of the wavelet representation for denoising signals. This optimality is in the sense that wavelet-based estimators minimize the maximum L^2-error for inhomogeneous regular functions perturbed by Gaussian white noise. We have chosen the variance of the total vorticity instead of the variance of the noise, which gives the threshold T

TABLE I. Statistical properties of the vorticity and velocity fields for CVS-wavelet and POD-Fourier.

Decomposition		CVS-wavelet		POD-Fourier	
Quantity	total	coherent–incoherent		large scale–small scale	
% of coefficients	100	2.9	97.1	2.9	97.1
Enstrophy	4895	3872	1023	3455	1440
% of enstrophy	100	79.1	20.9	70.6	29.4
Vorticity skewness	−0.048	−0.056	0.000	−0.041	−0.002
Vorticity flatness	8.7	9.6	4.8	6.1	9.6
Energy	43.0	42.6	0.2	42.7	0.3
% of energy	100	99.1	0.47	99.3	0.7
Velocity skewness	0.051	0.052	0.000	0.053	0.003
Velocity flatness	2.9	2.9	3.4	2.8	6.8

$=(\frac{4}{3}Z\log N)^{1/2}$, where $Z=\frac{1}{2}\langle\boldsymbol{\omega},\boldsymbol{\omega}\rangle$ is the total enstrophy and N is the resolution proportional to R_λ. Notice that this threshold does not require any adjustable parameter.

We then compute the modulus of the wavelet coefficients

$$|\tilde{\boldsymbol{\omega}}^{\mu}_{j,i_x,i_y,i_z}|=\left(\sum_{n=1}^{3}[\tilde{\omega}^{\mu}_{j,i_x,i_y,i_z}]^2_n\right)^{1/2}. \tag{1}$$

The coherent vorticity is then reconstructed from the wavelet coefficients whose modulus is larger than the threshold T, while the incoherent vorticity is reconstructed from the remaining wavelet coefficients. The two fields thus obtained, $\boldsymbol{\omega}_C$ and $\boldsymbol{\omega}_I$, are orthogonal, which ensures the decomposition of the total enstrophy into $Z=Z_C+Z_I$.

Biot–Savart's relation $\boldsymbol{V}=\nabla\times(\nabla^{-2}\boldsymbol{\omega})$ is used to reconstruct the coherent and incoherent velocities, $\boldsymbol{V}_C(\boldsymbol{x})$ and $\boldsymbol{V}_I(\boldsymbol{x})$, from the corresponding coherent and incoherent vorticities. Since wavelets are ''almost'' eigenfunctions of singular Calderon–Zygmund kernels,[23] such as Biot–Savart's kernel, the two velocity fields are quasi-orthogonal and the total energy is decomposed into $E=E_C+E_I+\epsilon$, where $E=\frac{1}{2}\langle\boldsymbol{V},\boldsymbol{V}\rangle$ and $\epsilon<0.5\%E$ (Table I).

C. Divergence problem

The continuous wavelet transform commutes with the divergence operator, but not its discrete version, which loses the translational invariance property of the continuous transform.[10] Therefore, since the vector-valued wavelet basis we have chosen here is not divergence-free, the CVS decomposition does not yield coherent and incoherent vorticity fields that are perfectly solenoidal. The same problem also occurs for vortex methods[24] and for large eddy simulations (LES) using filters other than the Fourier cutoff filter. In spite of that, the corresponding coherent and incoherent velocity fields are divergence-free, since they are reconstructed using Biot–Savart's relation.

There are several ways to insure that the coherent and incoherent vorticities remain solenoidal:

(i) use divergence-free vector-valued wavelets;[25–27]
(ii) decompose $\boldsymbol{\omega}$ into $\boldsymbol{\omega}=\boldsymbol{\omega}_{\mathrm{div}=0}+\nabla\phi$ and calculate ϕ by taking the divergence of $\boldsymbol{\omega}$, which yields the Poisson equation $\nabla^2\phi=\nabla\cdot\boldsymbol{\omega}$;
(iii) apply the previous decomposition, not to the solution, but to the wavelet basis itself. This can be done as a pre-calculation, since the wavelet decomposition is a linear transformation.

In Fig. 2 we have compared the one-dimensional isotropic enstrophy spectrum, $Z(k)=\frac{1}{2}\int_{k=|\boldsymbol{k}|}|\hat{\boldsymbol{\omega}}(\boldsymbol{k})|^2d\boldsymbol{k}$ where $\hat{\boldsymbol{\omega}}(\boldsymbol{k})=\int\boldsymbol{\omega}(\boldsymbol{x})e^{-i\boldsymbol{k}\cdot\boldsymbol{x}}d\boldsymbol{x}$, of the coherent flow with and without imposing the divergence-free condition. We have checked that the non-solenoidal contribution remains below 2.9% of the total coherent enstrophy and only appears in the dissipative range. The same result holds for the incoherent enstrophy. The fact that there is no divergent contribution in the inertial range guarantees that the nonlinear dynamics, and therefore the flow evolution, is not affected by the divergent contribution of vorticity. Therefore, we do not think that it is necessary to implement one of the procedures mentioned above to force the coherent and incoherent vorticity fields to remain perfectly solenoidal.

III. APPLICATION OF THE CVS DECOMPOSITION

A. Comparison with the POD-Fourier decomposition

The proper orthogonal decomposition (POD),[28] introduced in the 1940s by Kosambi, Loève, and Karhunen, has

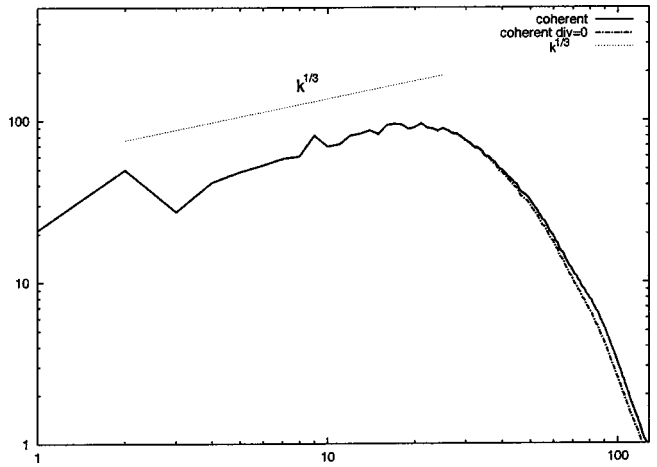

FIG. 2. Comparison between the enstrophy spectrum of the coherent vorticity with (dashed line) and without (full line) the divergence-free condition.

been applied to turbulence by Obukhov and Lumley.[29] It is also called Karhunen–Loève (KL) decomposition, principal component analysis (PCA), empirical orthogonal functions (EOF) or singular value decomposition (SVD), depending on its domain of application. It computes the two-point correlation tensor of an ensemble of realizations, then diagonalizes it and retains only the eigenmodes which have the largest eigenvalues. It yields the best basis for this ensemble of realizations with respect to the L^2-norm. The retained modes are defined *a posteriori* for all realizations, as those containing, on average, the most variance. Thus, the decomposition is linear, as the selection of the retained modes does not depend on each realization.

In contrast, the CVS-wavelet decomposition performs the selection of the retained modes *a priori*, i.e., without knowing all the flow realizations, by selecting from an orthonormal wavelet basis the functions whose amplitudes have the strongest values. Hence, the selection procedure is nonlinear, as the retained basis functions depend on each flow realization. For the time-integration, CVS retains at time t the active wavelets whose modulus is larger than the threshold T, plus their neighbors in wavelet space, which are necessary to compute the flow evolution from t to $(t+\Delta t)$. After computing the solution at time $(t+\Delta t)$ using the wavelets selected at time t, the coefficients whose modulus has become smaller than the threshold T are discarded. Subsequently, new active wavelets, i.e., those whose moduli have become larger than T plus their neighbors, are added to define the computational basis at time $(t+\Delta t)$. This selection of the active wavelets is nonlinear, because it depends on the flow realization at time t, and on the direction of the transfers in wavelet space between $(t-\Delta t)$ and t, used to select the neighbor wavelets added to the active wavelet set: for more details see Refs. 5 and 7.

For a homogeneous and isotropic flow, such as the one studied here, the two-point correlation tensor is invariant under translation and rotation: therefore POD yields a Fourier basis whose modes are sorted by decreasing order of wavenumber $k=|\boldsymbol{k}|$. This is a particular case of a low-pass filter used in LES, where the large scale modes are deterministically computed, while the effect of the small scale modes (the subgrid scale contribution) on the resolved large scale modes is modeled.

B. Application to a homogeneous turbulent flow

We consider a three-dimensional homogeneous isotropic turbulent flow, computed by direct numerical simulation (DNS) using a classical pseudo-spectral code at resolution $N=256^3$, which corresponds to a Reynolds number based on the Taylor microscale $R_\lambda=168$. The computation has been initialized with a Gaussian random vorticity field, and performed until a statistically stationary state has been reached. Figure 4 shows the modulus of the vorticity fluctuations of the total flow (only a 64^3 sub-cube is shown to get a more precise visualization). It exhibits elongated and distorted vortex tubes, as previously observed in both laboratory and numerical experiments.[30–32]

We compare CVS-wavelet and POD-Fourier applied to the same flow realization, and for the same compression rate. Let us first consider the CVS decomposition. After expanding the three components of the vorticity field in an orthonormal wavelet series, we calculate $\frac{1}{2}|\tilde{\boldsymbol{\omega}}^{\mu}_{j,i_x,i_y,i_z}|^2$ using (1) to get the enstrophy retained by each wavelet. Subsequently, we sort the N wavelets by decreasing order of retained enstrophy, compute their partial sum, and plot the percentage of retained enstrophy versus the percentage of retained wavelets to obtain the compression curve of the wavelet basis for this flow realization (Fig. 3).

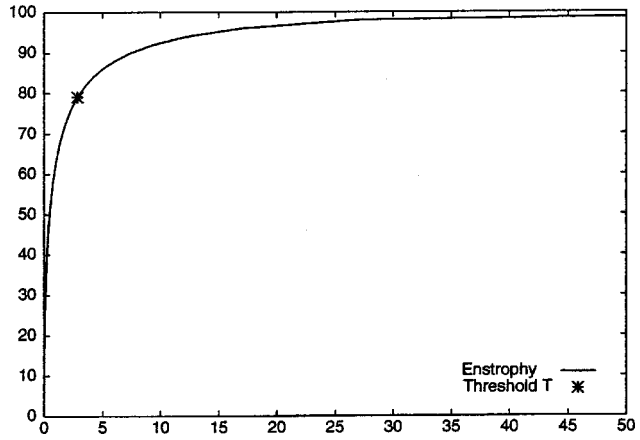

FIG. 3. Compression curve for the CVS decomposition: % of retained enstrophy versus % of retained wavelets (the star corresponds to the threshold T).

This curve shows that very few wavelets contain most of the enstrophy, and that, if more than $10\%N$ wavelets are kept, it saturates rapidly. This saturation corresponds to a quasi-equipartition of the enstrophy among the $90\%N$ weakest wavelet modes, which is characteristic of random fields. In Fig. 3 we indicate by a star the threshold T we use, which retains 2.9% of the wavelet coefficients and 79% of the enstrophy. The coherent vorticity $\boldsymbol{\omega}_C$ is then reconstructed from the wavelet coefficients whose moduli are above T, and the incoherent vorticity $\boldsymbol{\omega}_I$ is the remainder. Using Biot–Savart's relation, we also compute the corresponding coherent velocity, $\boldsymbol{V}_C=\nabla\times(\nabla^{-2}\boldsymbol{\omega}_C)$, and incoherent velocity, $\boldsymbol{V}_I=\nabla\times(\nabla^{-2}\boldsymbol{\omega}_I)$.

We now perform the POD-Fourier decomposition of the same flow realization, and for the same compression rate as before. As noted above, the POD basis for such a homogeneous and isotropic flow is the Fourier basis, whose modes are sorted in decreasing order of wavenumber $k=|\boldsymbol{k}|$. We thus expand the vorticity field in Fourier space and retain the $2.9\%N$ modes for which the wavenumber k is smaller than the cut-off wavenumber $k_c=48$. It does not matter whether we decompose the vorticity field or the velocity field, as the Fourier basis diagonalizes the inverse curl operator (Biot–Savart's kernel).

C. Comparison of physical space reconstruction

Figure 5 (top) displays the modulus of the coherent (left) and incoherent (right) vorticity fluctuations resulting from the CVS decomposition, while Fig. 5 (bottom) displays the modulus of the large scale (left) and small scale (right) vor-

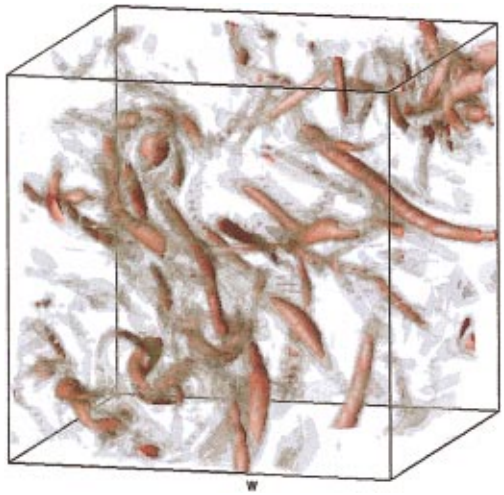

FIG. 4. (Color) Modulus of vorticity of the total flow (isosurfaces $|\boldsymbol{\omega}|=3\sigma$, 4σ, 5σ where $\sigma^2=2Z$ is the variance of the vorticity fluctuations).

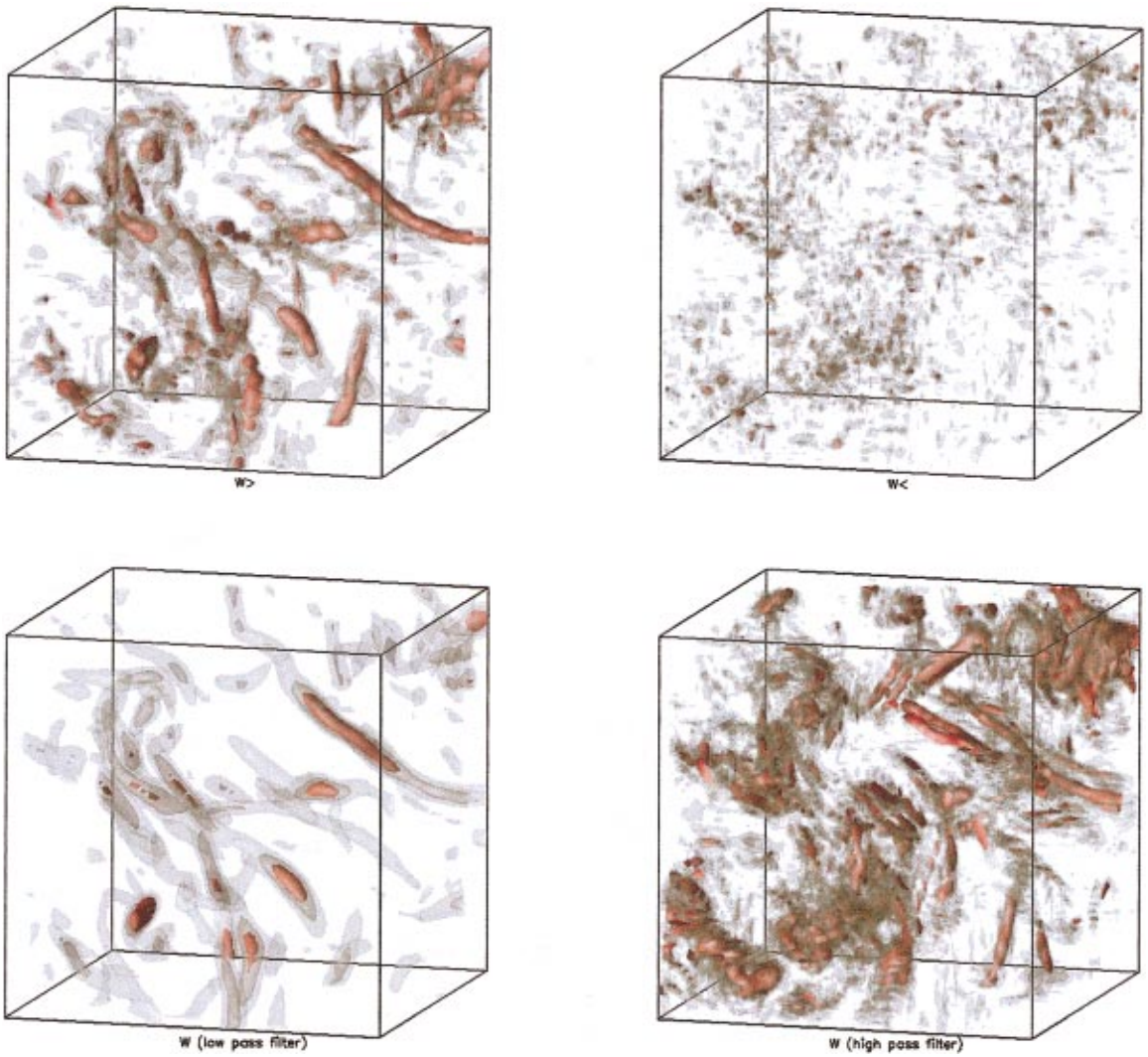

FIG. 5. (Color) Comparison between CVS-wavelets (top) and POD-Fourier (bottom) compressions: Modulus of vorticity for the retained (left) and discarded (right) modes (isosurfaces $|\boldsymbol{\omega}|=3\sigma$, 4σ, 5σ, and $3/2\sigma$, 2σ, $5/2\sigma$, respectively). Top, left: coherent flow; top right: incoherent flow; bottom, left: large scale flow; bottom right: small scale flows.

ticity fluctuations resulting from POD or LES decompositions. Note that the values of the three iso-surfaces chosen for visualization (3σ, 4σ, and 5σ with $\sigma^2 = 2Z$ the variance of the vorticity fluctuations) are the same for the total, the coherent and the large scale vorticities, but they have been reduced by a factor of two for the incoherent and small scale vorticities whose fluctuations are much smaller.

In the coherent vorticity (Fig. 5, top, left), which corresponds to the modes retained by the CVS-wavelet decompostion, we recognize the same vortex tubes as those present in the total vorticity (Fig. 4). In contrast, the incoherent vorticity (Fig. 5, top, right), which corresponds to the discarded modes, is much more homogeneous and does not exhibit any coherent vortices. Hence, the CVS decomposition extracts all the vortex tubes, whatever their scales. The resulting coherent flow is as intermittent as the total flow, while the discarded incoherent flow is structureless and non-intermittent. This enables us to model quite easily the effect of the incoherent flow onto the coherent flow, as discussed in Ref. 5.

In the large scale vorticity (Fig. 5, bottom, left), which corresponds to the modes retained by the POD-Fourier or LES decompositions, we observe most of the vortex tubes. But, when we compare them with those retained in the coherent vorticity (Fig. 5, top, left), we find that they are weaker and much smoother, since their small scale contribution has been removed. As a consequence, the small scale vorticity (Fig. 5, right) also exhibits coherent structures, similar to those in the total vorticity (Fig. 4). Therefore the small scale flow remains intermittent and exhibits localized bursts, which correspond to the small scale contribution of the vortex tubes, whose effect on the large scale flow would be difficult to model.

D. Comparison of statistics

In Table I we show that only 2.9% wavelet modes correspond to the coherent flow, which retains 99% of the energy and 79% of the enstrophy, while the remaining 97.1% incoherent modes contain only 0.47% of the energy and 21% of the enstrophy. For the same compression rate, POD-Fourier retains about the same amount of energy as CVS-wavelet, but slightly less enstrophy (71% instead of 79%Z).

Figure 6 (top) shows the PDF of the vorticity in semilogarithmic coordinates. For CVS (left), the coherent vorticity presents a very similar stretched exponential behavior, including the tails, as the total vorticity, with flatness 9.6 instead of 8.7 (Table I). The incoherent vorticity has an exponential PDF, with much weaker tails, and flatness 4.8. For POD-Fourier or LES (right), the PDF of the large scale vorticity is exponential with flatness 6.1, while it is a stretched exponential with flatness 9.6 for the small scale vorticity. They both have about the same range of variation, which is not the case for the CVS-wavelet decomposition, where the extrema of the incoherent vorticity are 3.6 times weaker than those of the coherent vorticity. This is another indication of the difficulty to model the effect of the small scales on the large scales.

Figure 6 (middle) shows the velocity PDF in semilogarithmic coordinates for both CVS (left) and POD (right). The skewness of the total velocity and vorticity is about zero, and both CVS and POD preserve this property (Table I). We observe that the coherent velocity has the same Gaussian distribution as the total velocity, with flatness 2.9, and the incoherent velocity also remains almost Gaussian, with flatness 3.4, but its variance is 185 times smaller (Table I). In contrast, the velocity PDF for POD (Fig. 6, middle, right) shows that, although the large scale contribution is Gaussian with flatness 2.8, the small scale contribution exhibits a stretched exponential behavior, with flatness 6.8. This non-Gaussianity of the small scale flow has already been noticed in laboratory and numerical experiments.[33] As a consequence, the modeling issue will be more difficult for POD or LES than for CVS, whose incoherent velocity is almost Gaussian and has a strongly reduced variance.

The corresponding one-dimensional isotropic energy spectra, $(E(k) = \frac{1}{2}\int_{k=|\boldsymbol{k}|} |\boldsymbol{V}(\boldsymbol{k})|^2 d\boldsymbol{k}$, are plotted on Fig. 7 (top), where we have indicated the cut-off wavenumber $k_c = 48$ separating the large scale and small scale contributions of POD-Fourier or LES. We observe that the spectrum of the coherent energy is identical to the spectrum of the total energy all along the inertial range. This implies that the vortex tubes are responsible for the $k^{-5/3}$ energy scaling, which corresponds to a long-range correlation between them. In contrast, the incoherent energy has a scaling close to k^2, which corresponds to an energy equipartition between all wavevectors $\boldsymbol{k}$, since the one-dimensional isotropic spectrum is obtained by integrating energy in three-dimensional $\boldsymbol{k}$-space over two-dimensional shells $k = |\boldsymbol{k}|$. The incoherent velocity field is therefore spatially decorrelated, which is consistent with the observation that incoherent vorticity is structureless and homogeneous (Fig. 5, top, right). Thus, we have found that the incoherent energy is uniformly distributed in Fourier (Fig. 7, top), wavelet (Fig. 3), and physical (Fig. 5, top, right) spaces. This gives strong evidence of its random nature, since by definition noise cannot be local in any basis. In contrast, POD-Fourier does not exhibit such decorrelation, since its small scale contribution is not uniformly distributed, neither in Fourier space, nor in physical space where it exhibits inhomogeneities (Fig. 5, bottom, right).

To check the dynamical behavior of the coherent and incoherent flows we compute their energy transfers in wavenumber space. Figure 7 (bottom) shows that the direct energy transfers, from large to small scales, are the same for the coherent and total flows. This proves that the coherent flow triggers all nonlinear interactions, which are fully resolved by the CVS filter. Therefore, there is no need to parametrize the effect of the discarded incoherent modes on the retained coherent modes. This is no more the case for the large scale flow, whose energy transfers present a strong accumulation near the cut-off scale k_c. A subgrid parametrization is then necessary to extract the energy coming from the large scales which otherwise piles up at k_c.

From these observations, we propose the following scenario to interpret the turbulent cascade. The coherent energy is nonlinearly transferred towards small scales by the nonlinear interactions between vortex tubes, i.e., their stretching, folding and twisting. In the meantime these nonlinear inter-

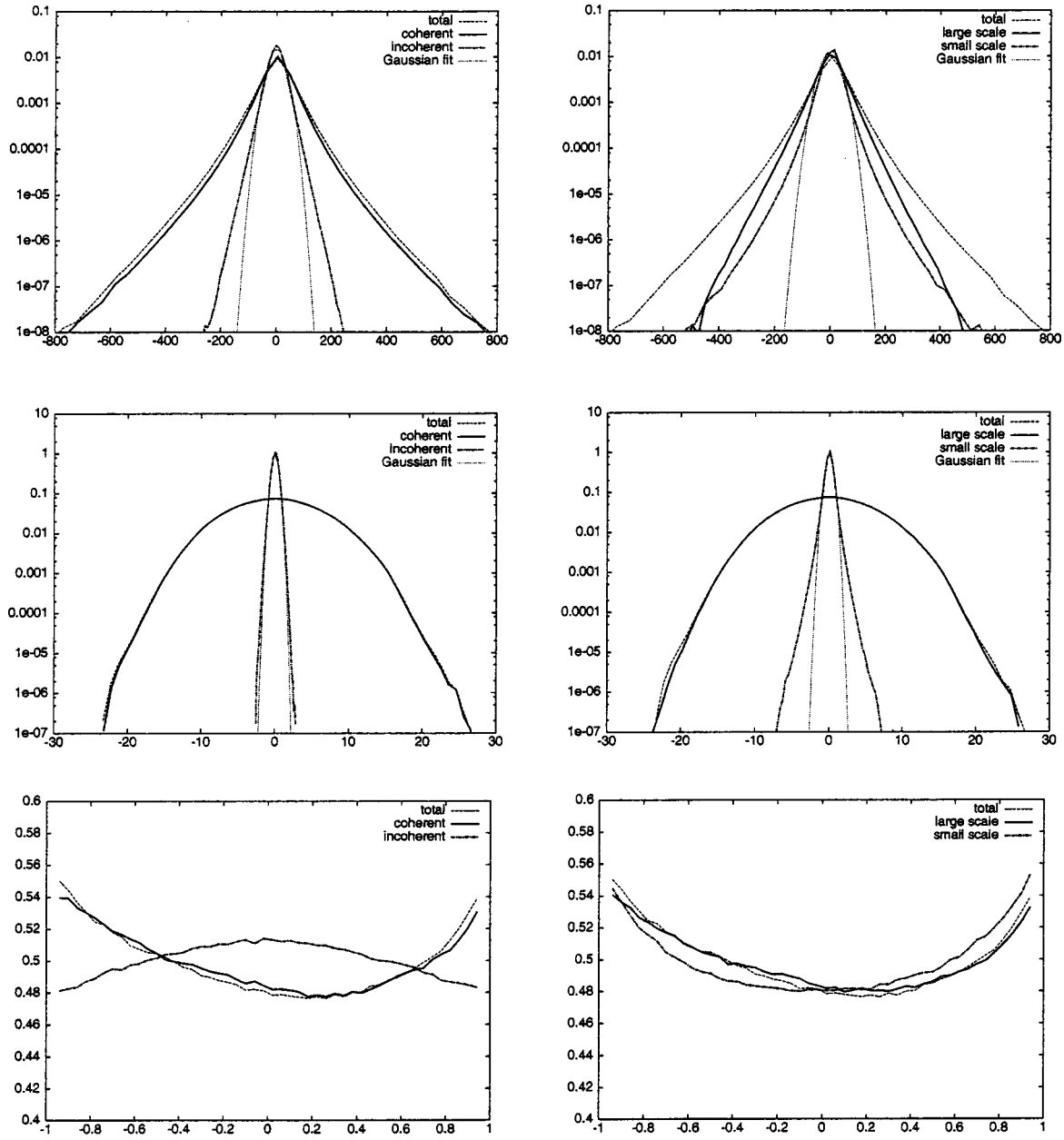

FIG. 6. Comparison between CVS-wavelet (left) and POD-Fourier (right) compressions: PDFs of vorticity (top), velocity (middle) and relative helicity (bottom).

actions also produce incoherent energy at all scales (in a way analogous to white noise emission), which is only dissipated at the smallest scales by molecular viscosity. We conjecture that the coherent flow is dynamically active, while the incoherent flow is slaved to it, being only passively advected, strained and mixed by the coherent vortex tubes. In contrast, the small scale flow, discarded by the POD-Fourier or LES filter, is not slaved but remains dynamically active due to the small scale contribution of the coherent tubes, which may cause backscatter as observed by Ref. 34, i.e., there may be some energy transfers towards large scales. This is another evidence of the modeling problem that POD-Fourier or LES may encounter.

E. Comparison of the geometrical alignment between velocity and vorticity

Since the CVS filtering is based on *a priori* denoising, without any dynamical assumption or pattern recognition hypotheses about the vortex tubes, we now check *a posteriori* that we have actually extracted them. Following Ref. 9 they can be described as local steady solutions of the Euler equation where the nonlinearity is locally depleted, which happens, in particular, where vorticity and velocity vectors become aligned. This geometrical alignment maximizes the relative helicity $h = \boldsymbol{V}\cdot\boldsymbol{\omega}/(|\boldsymbol{V}||\boldsymbol{\omega}|)$ and is called Beltramization.[35]

In Fig. 6 (bottom, left) we show that the coherent flow

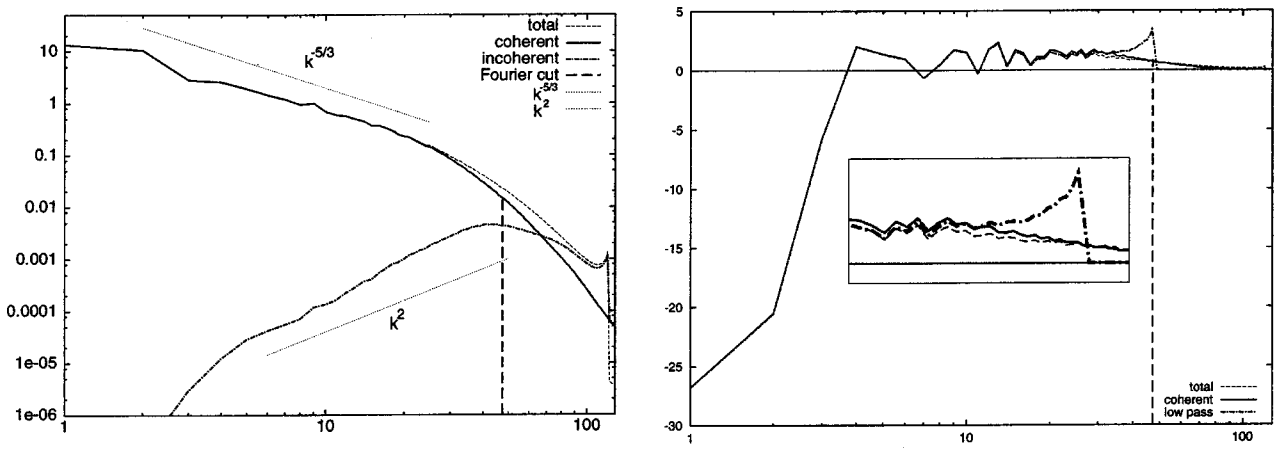

FIG. 7. Energy spectra $E(k)$ (top) for the total, coherent and incoherent flows, and energy transfers $d_t E(k)$ (bottom) for the total, coherent (CVS) and large scale (POD) flows. The vertical line corresponds to the Fourier cut-off wavenumber $k_c = 48$. Inset: Zoom around k_c (from $k = 20$ to 50).

exhibits the same tendency towards local Beltramization as the total flow, which is characterized by the two maxima observed in the PDF of the relative helicity for $h = +1$ (alignment) and $h = -1$ (anti-alignment). In contrast, the incoherent flow is more evenly distributed, with a maximum at $h = 0$ which indicates a tendency towards local two-dimensionalization. This observation, together with the evidence of strong dissipation in the incoherent flow (Fig. 7, top), agrees with the remark of Moffatt:[35] "*Euler flows contain blobs of maximal helicity (positive or negative) which may be interpreted as 'coherent structures,' separated by regular surfaces on which vortex sheets, the site of strong viscous dissipation, may be located.*" Following this picture, we conjecture that the CVS coherent flow is dominated by three-dimensional vortex tubes which tend to maximize helicity, while the incoherent flow is made of two-dimensional vortex sheets which tend to maximize dissipation.

The POD-Fourier or LES decompositions differ from the CVS-wavelet decomposition since they do not disentangle components exhibiting different geometrical alignments. We observe that both the total, large scale and small scale flows exhibit the same PDF of the relative helicity (Fig. 6, bottom, right). This comes from the fact that each vortex tube in the total flow contributes to both the large and small scales flows.

IV. CONCLUSION

We have shown that the CVS decomposition, based on the nonlinear filtering of the wavelet coefficients of vorticity, is an efficient tool for extracting coherent vortices out of turbulent flows. We have applied it to a three-dimensional homogeneous isotropic turbulent flow, computed at resolution $N = 256^3$, which is decomposed into two orthogonal components: A low-dimensional ($2.9\%N$) coherent flow, made of vortex tubes, which is long-range correlated with a $k^{-5/3}$ energy spectrum, and a large-dimensional ($97.1\%N$) incoherent flow, which is random, decorrelated and has a Gaussian velocity PDF. For the same compression rate, the POD, which degenerates for this homogeneous isotropic case in the Fourier basis, does not extract the vortex tubes equally well. The small scale contribution of the coherent vortices extracted with the POD-Fourier remains in the small scale flow, resulting in a stretched exponential PDF of velocity. Therefore, modeling the effect of the discarded modes on the resolved modes is easier to perform with CVS than with POD-Fourier or LES.

In order to avoid a common misunderstanding, we stress that:

(i) the incoherent flow is not only small scale, but multiscale, because its energy is spread over all scales as a white noise;
(ii) the coherent flow is not only large scale, but multiscale, although it dominates the large scales due to its long-range correlation. Moreover, the coherent flow also contains small scales associated with the stretched and distorted vortex tubes.

As a consequence, two different kinds of motion contribute to the small scales:

(i) incoherent motions which, under the effect of the strong mixing exerted by the coherent vortex tubes, have already reached a statistical equilibrium, characterized by the equipartition of energy and the Gaussianity of the velocity PDF;
(ii) coherent motions, dominated by the nonlinear interactions between vortex tubes which generate small scales by their mutual stretching, folding and twisting. Those are not yet in statistical equilibrium, since they are long-range correlated and their velocity PDF is non-Gaussian.

We conjecture that only the coherent motions are dynamically active and trigger the nonlinear dynamics and the resulting energy cascade. The incoherent background flow, produced by the nonlinear interactions between the coherent vortex tubes, is passively advected and strained by them. This straining inhibits any instability to develop in the incoherent flow, and results in a strong mixing which leads to the dissipation of incoherent energy by molecular viscosity. Since the incoherent motions are slaved to the coherent flow,

their effect remains negligible. Therefore, discarding at each time step the incoherent energy produced by the nonlinear vortex interactions is a way to model turbulent dissipation.[5] In addition a wavelet forcing technique, proposed in Ref. 36, can be used, as illustrated in Ref. 5 for a two-dimensional mixing layer.

Although we have considered here a homogeneous isotropic turbulent flow, the previous observations concerning CVS remain also valid for inhomogeneous turbulent flows,[13,19] as long as they contain vortices which are advected by the mean velocity field induced by all the other vortices (e.g., wakes, shear layers, boundary layers). For such inhomogeneous flows there is often a local invariance by translation due to the vortex advection. For these inhomogeneous cases a nonlinear method, such as CVS, remains more appropriate to extract the coherent vortices in each flow realization than a linear method such as POD or LES.

In conclusion, we think that the classical strategy of expanding the flow in a given basis and truncating the series to a fixed number of resolved modes can be improved. One should keep in mind that DNS and LES of turbulent flows integrate only one flow realization at a time, and that the statistics are computed afterwards by averaging several realizations. Therefore, POD, which is by construction the best basis to represent an ensemble of flow realizations with a reduced number of modes, is not necessarily the best decomposition for computing the evolution of each flow realization. CVS offers a nonlinear strategy which adapts the number of resolved modes to each flow realization, by projecting it, at each time step, onto an orthonormal wavelet basis and retaining only the strongest wavelet coefficients. Thus, CVS makes it possible to compute all degrees of freedom which contribute to the flow nonlinearity, i.e., the coherent modes, whatever their scale, while the remaining degrees of freedom, i.e., the incoherent modes, are discarded to model turbulent dissipation. The method actually combines an Eulerian projection of the solution with a Lagrangian procedure for the adaption of the computational basis.[5,6] The next step is to perform three-dimensional CVS computations of turbulent flows. Preliminary results have been obtained for a 3D temporally developing turbulent mixing layer.[37]

ACKNOWLEDGMENTS

We are grateful to Bud Homsy, Konrad Bajer, and Joel Ferziger for useful comments. M.F. and K.S. thankfully acknowledge the hospitability of the Center for Turbulence Research, NASA-Ames and Stanford University, where this work has been done during the Summer Program 2000. G.P. acknowledges the grant from the European Community, TMR program on ''Wavelets and numerical simulation,'' Contract No. FMRX-CT98-0184.

[1] M. Farge, K. Schneider, G. Pellegrino, A. A. Wray, and R. S. Rogallo, ''CVS decomposition of 3D homogeneous turbulence using orthogonal wavelets,'' *CTR Summer Program 2000* (NASA/Stanford University, Stanford, CA, 2000), pp. 305–317.

[2] H. L. Dryden, ''Recent advances in the mechanics of boundary layer flow,'' Adv. Appl. Mech. **1**, 1 (1948).

[3] M. Farge, K. Schneider, and N. Kevlahan, ''Non-Gaussianity and coherent vortex simulation for two-dimensional turbulence using an adaptive orthonormal wavelet basis,'' Phys. Fluids **11**, 2187 (1999).

[4] K. Schneider and M. Farge, ''Numerical simulation of temporally growing mixing layer in an adaptive wavelet basis,'' C. R. Acad. Sci., Ser. IIb: Mec., Phys., Chim., Astron. **328**, 263 (2000).

[5] M. Farge and K. Schneider, ''Coherent vortex simulation (CVS), a semi-deterministic turbulence model using wavelets,'' Flow, Turbul. Combust. **66(4)**, 393 (2001).

[6] K. Schneider, N. Kevlahan, and M. Farge, ''Comparison of an adaptive wavelet method and nonlinearly filtered pseudo-spectral methods for two-dimensional turbulence,'' Theor. Comput. Fluid Dyn. **9**, 191 (1997).

[7] K. Schneider and M. Farge, ''Wavelet approach for modeling and computing turbulence,'' *Lecture Series 1998-05 Advances in Turbulence Modelling* (von Karman Institute for Fluid Dynamics, Bruxelles, 1998), pp. 1–132.

[8] K. Schneider and M. Farge, ''Adaptive wavelet simulation of a flow around an impulsively started cylinder using penalization,'' Appl. Comput. Harm. Anal. **12**, 374 (2002).

[9] M. Farge, G. Pellegrino, and K. Schneider, ''Coherent vortex extraction in 3D turbulent flows using orthogonal wavelets,'' Phys. Rev. Lett. **87**, 054501 (2001).

[10] M. Farge, ''Wavelet transforms and their applications to turbulence,'' Annu. Rev. Fluid Mech. **24**, 395 (1992).

[11] M. Farge and G. Rabreau, ''Transformée en ondelettes pour détecter et analyser les structures cohérentes dans les écoulements turbulents bidimensionnels,'' C. R. Acad. Sci., Ser. IIb: Mec., Phys., Chim., Astron. **307**, 433 (1988).

[12] M. Farge, Y. Guezennec, C. M. Ho, and C. Meneveau, ''Continuous wavelet analysis of coherent structures,'' *CTR Summer Program 1990* (NASA/Stanford University, Stanford, CA, 1990), pp. 331–343.

[13] K. Schneider, M. Farge, G. Pellegrino, and M. S. Rogers, ''CVS filtering of 3D turbulent mixing layers using orthogonal wavelets,'' *CTR Summer Program 2000* (NASA/Stanford University, Stanford, CA, 2000), pp. 319–330.

[14] J. Bass, ''Les fonctions aléatoires et leur interprétation mécanique,'' Rev. Sci. **83**, 3 (1945).

[15] M. Farge, E. Goirand, Y. Meyer, F. Pascal, and V. M. Wickerhauser, ''Improved predictability of two-dimensional turbulent flows using wavelet packet compression,'' Fluid Dyn. Res. **10**, 229 (1992).

[16] M. L. Wickerhauser, M. Farge, E. Goirand, E. Wesfreid, and E. Cubillo, ''Efficiency comparison of wavelet packet and adapted local cosine bases for compression of a two-dimensional turbulent flow,'' *Wavelets: Theory, Algorithms and Applications*, edited by C. Chui *et al.* (Academic, New York, 1992), pp. 509–531.

[17] D. Donoho, ''Unconditional bases are optimal bases for data compression and statistical estimation,'' Appl. Comput. Harmon. Anal. **1**, 100 (1993).

[18] D. Donoho and I. Johnstone, ''Ideal spatial adaption via wavelet shrinkage,'' Biometrics **81**, 425 (1994).

[19] M. Farge, A. Azzalini, A. Mahalov, B. Nicolaenko, F. Tse, G. Pellegrino, and K. Schneider, ''Vortex tubes in shear-stratified turbulence,'' *IUTAM Symposium on Tubes, Sheets and Singularities*, edited by K. Bajer and K. Moffatt (Kluwer Academic, Dordrecht, 2003), pp. 217–228.

[20] J. Lewalle, J. Delville, and J.-P. Bonnet, ''Decomposition of mixing layer turbulence into coherent structures and background fluctuations,'' Flow, Turbul. Combust. **64**, 301 (2000).

[21] J.-P. Bonnet and J. Delville, ''Review of coherent structures in turbulent free shear flows and their possible influence on computational methods,'' Flow, Turbul. Combust. **66**, 333 (2001).

[22] I. Daubechies, *Ten Lectures on Wavelets*, CBMS-NSF Conferences in Applied Mathematics, Vol. 61 (SIAM, Philadelphia, 1992).

[23] Y. Meyer, *Wavelets and Operators* (Cambridge University Press, Cambridge, 1992).

[24] G. S. Winckelmans, ''Some progress in large-eddy simulation using the 3D vortex particle method,'' *CTR Annual Research Briefs* (NASA/Stanford University, Stanford, CA, 1995), pp. 391–415.

[25] G. Battle and P. Federbush, ''Divergence-free vector wavelets,'' Michigan Math. J. **40(1)**, 181 (1993).

[26] P. G. Lemarié, ''Analyses multirésolutions non orthogonales, commutation entre projecteurs de dérivation et ondelettes à divergence nulle,'' Revista Mat. Iberoamericana **8**, 221 (1992).

[27] P. G. Lemarié-Rieusset, ''Un théorème d'existence pour les ondelettes vecteurs à divergence nulle,'' C. R. Acad. Sci. Paris **319**, 811 (1994).

[28] G. Berkooz, P. Holmes, and J. L. Lumley, ''The proper orthogonal decomposition in the analysis of turbulent flows,'' Annu. Rev. Fluid Mech. **25**,

539 (1993).
[29]J. Lumley, *Stochastic Tools in Turbulence* (Cambridge University Press, Cambridge, 1972).
[30]S. Douady, Y. Couder, and M. E. Brachet, ''Direct observation of the intermittency of intense vorticity filaments in turbulence,'' Phys. Rev. Lett. **67**, 983 (1991).
[31]J. Jimenez and A. A. Wray, ''The structure of intense vorticity in isotropic turbulence,'' J. Fluid Mech. **255**, 65 (1993).
[32]A. Vincent and M. Meneguzzi, ''The spatial structure and statistical properties of homogeneous turbulence,'' J. Fluid Mech. **225**, 1 (1991).
[33]A. Tsinober, *An Informal Introduction to Turbulence*, *Fluid Mechanics and its Applications*, Vol. 63 (Kluwer Academic, Dordrecht, 2001).
[34]J. A. Domaradski and R. Rogallo, ''Local energy transfer and nonlocal interaction in homogeneous, isotropic turbulence,'' Phys. Fluids A **2**, 413 (1990).
[35]H. K. Moffatt, ''Magnetostatic equilibria and analogous Euler flows of arbitrary complex topology,'' J. Fluid Mech. **150**, 359 (1985).
[36]K. Schneider and M. Farge, ''Wavelet forcing for numerical simulation of two-dimensional turbulence,'' C. R. Acad. Sci., Ser. IIb: Mec., Phys., Chim., Astron. **325**, 263 (1997).
[37]G. Pellegrino, K. Schneider, and M. Farge, ''Coherent vortex simulation of a three-dimensional temporally developing turbulent mixing layer,'' *Advances in Turbulence IX*, edited by I. P. Castro, P. E. Hancock, and T. G. Thomas (CIMNE, Barcelona, 2002), pp. 341–344.